LANGMUIR Article
Cite This: Langmuir 2019, 35, 9483−9492
pubs.acs.org/Langmuir

Small-Angle X-ray Scattering Studies on the Structure of Disc-Shaped Bicelles Incorporated with Neutral PEGylated Lipids

Ching-Hsun Yang,[†] Tsang-Lang Lin,*[,†] and U-Ser Jeng[‡,§]

[†]Department of Engineering and System Science, National Tsing Hua University, 101, Section 2, Kuangfu Road, Hsinchu, Taiwan 30013, Republic of China

[‡]National Synchrotron Radiation Research Center, No. 101, Hsin-Ann Road, Hsinchu Science Park, Hsinchu, Taiwan 30076, Republic of China

[§]Department of Chemical Engineering, National Tsing Hua University, 101, Section 2, Kuangfu Road, Hsinchu, Taiwan 30013, Republic of China

Supporting Information

ABSTRACT: In this study, small-angle X-ray scattering (SAXS) is successfully employed to investigate the structure of the DPPC/diC7PC disc-shaped bicelles incorporated with different amounts of C16-PEG2000-Ceramide lipids. The incorporation of the C16-PEG2000-Ceramide lipids could provide an antifouling capability to the bicelle for biomedical applications. However, traditionally it is believed that most of the incorporated PEGlylated lipids should lie in the rim of the disc-shaped bicelle. In this study, high sensitivity SAXS reveals the distribution of the added C16-PEG2000-Ceramide lipids in both the planar region and in the rim of the bicelle. The PEG brushes of C16-PEG2000-Ceramide lipids form a second shell outside the lipid headgroup shell of the bicelle. A double shell disc bicelle model is used in analyzing the SAXS data. The lipid density of C16-PEG2000-Ceramide in the rim is found to be about 1.7 times the C16-PEG2000-Ceramide lipid density in the planar region for all three C16-PEG2000-Ceramide concentrations, 1, 2, and 3 mM. Moreover, the bicelle core radius can be predicted well using the actual molecular ratio of lipids in the planar region to the lipids in the rim of the bicelles in the model calculation.

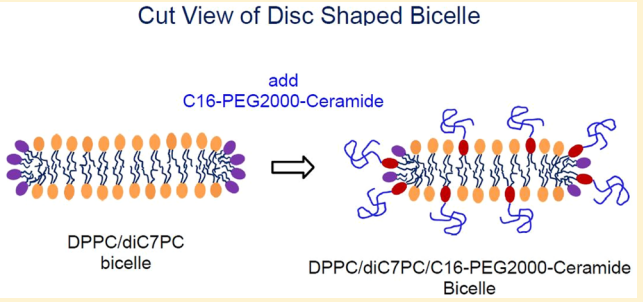

INTRODUCTION

Bicelles refer to a disc-shaped aggregate which consists of a bilayer core formed by long-chain lipids (fatty acid chain length of 14 carbons or longer) and a rim region typically formed by short-chain lipids (fatty acid chain length of 6−8 carbons).[1−6] Long-chain lipids typically form unilamellar or multilamellar vesicles (curved bilayers) while short-chain lipids usually form globular or short rod-like micelles.[7−10] Mixing the long-chain lipids with short-chain lipids at suitable ratios, for example, a DPPC/diC7PC ratio roughly between 1 and 5, could spontaneously form disc-shaped bicelles in aqueous solution at room temperature.[5] Here, DPPC is the long-chain lipid, 1,2-dipalmitoyl-*sn*-glycero-3-phosphocholine, and the diC7PC is the short-chain lipid, 1,2-diheptanoyl-*sn*-glycero-3-phosphocholine, respectively. Highly monodisperse and stable bicelles can be formed with a typical diameter around 20 nm.[5,11] Bicelles are widely used as model systems to study the interaction of membrane and membrane-associated biomolecules by NMR and scattering methods.[12−18] The bilayer core of the bicelle resembles the cell membrane, and it can act as a membrane template for accommodating membrane proteins. The bicelles together with the inserted membrane proteins can be aligned in a magnetic field for studying the membrane protein's structural conformation and their functions by NMR.[18]

In recent years, bicelles are also used in many biomedical applications, such as drug delivery, gene therapy, etc.[19−24] Although the virus-mediated vectors have higher transfection efficiency for gene therapy, bicelles provide a biocompatible way to transfer genes, and using bicelles can also reduce the side effects caused by the immune system. For drug delivery, hydrophobic drugs can be loaded in the hydrophobic core of the bicelle, and there is a high cellular uptake via endocytosis for the drug loaded bicelles.[22] For biomedical applications, it is desirable to provide a steric property for bicelles. It has been well-developed for liposome drug delivery systems to incorporate PEGylated lipids to achieve steric effects.[25−31] The PEGylation is a way to attach polyethylene glycol (PEG) segments on the lipid headgroup to form the PEGylated lipids. With good biocompatibility and also low intrinsic toxicity, the PEGylated lipids are often used in preparing sterically stabilized liposomes to improve the therapeutic performance. The incorporation of PEGylated lipids in the liposome could

Received: March 14, 2019
Revised: June 20, 2019
Published: June 25, 2019

Downloaded via SYNCHROTRON RADIATION RESEARCH on January 10, 2020 at 07:49:59 (UTC).
See https://pubs.acs.org/sharingguidelines for options on how to legitimately share published articles.

© 2019 American Chemical Society

DOI: 10.1021/acs.langmuir.9b00756
Langmuir 2019, 35, 9483−9492

enhance the stability against blood plasma by protecting the liposome from endocytosis by the immune system, and the blood circulation time can be prolonged.[28,31]

Mixing the PEGylated lipids with only long-chain lipids could lead to greatly varied aggregation structures, from vesicles, to discs, to threads, depending on the preparation path, mixing ratios, and also the species of the long-chain lipids.[32−36] On the contrary, bicelles are much more stable, and it is expected that the incorporation of some PEGylated lipids should not destabilize the bicelle structure. The addition of PEGylated lipids to the bicelle should be able to provide a steric effect to the bicelle. However, how the added PEGylated lipids are distributed in the bicelle is still not clear, especially for the short-chain lipid stabilized bicelles incorporated with PEGylated lipids.[37] It is not clear whether the PEGylated lipids are mostly concentrated in the rim of the bicelle as is typically believed for the disc aggregates formed by mixing the PEGylated lipids with only the long-chain lipids,[32−36] or whether they would prefer to stay in the bilayer planar region since the rim of the bicelle is already occupied by the short-chain lipids. Another scenario is that the added PEGylated lipids are well-distributed both in the bilayer planar region as well as in the rim. If some of the incorporated PEGylated lipids are distributed in the bilayer planar region of the bicelle, it would be able to provide steric hindrance to the planar surface of the bicelle, such as to prevent or reduce the formation of stacked aggregates when cationic bicelles interact with DNA or other negatively charged polyelectrolytes.[38] Therefore, it is an important issue to clarify how the incorporated PEGylated lipids are distributed in the disc-shaped bicelle. It is also important to understand how the added PEGylated lipids affect the bicelle size. The bicelle size (diameter) is sensitive to the ratio of the number of lipids in the bilayer planar region to the number of lipids in the rim.[11,39] Thus, it matters whether the added PEGylated lipids lie in the bilayer planar region or in the rim. Small-angle X-ray scattering (SAXS) has been proven to be an effective technique in studying the bicelle structure.[5,11,40] SAXS is in particular sensitive to detect the headgroup layer of the bicelle and the brush layer of polymer micelles.[5,41,42] Especially, this study is focused on detecting the distribution of the added PEGylated lipids and the size changes when incorporating the PEGylated lipids. In the present study, SAXS is employed to investigate the structure of DPPC/diC7PC bicelles incorporated with different amounts of C16-PEG2000-Ceramide (*N*-palmitoyl-sphingosine-1-{succinyl-[methoxy(polyethylene glycol)$_{2000}$]}), which is a neutral PEGylated lipid. The chemical structure of C16-PEG2000-Ceramide is shown in Scheme 1. There are 45 oxyethylene units for the PEG2000. The scattering data are analyzed to reveal the detailed structure and the distribution of the added PEGylated lipids of the bicelles incorporated with different amounts of C16-PEG2000-Ceramide lipids.

Scheme 1

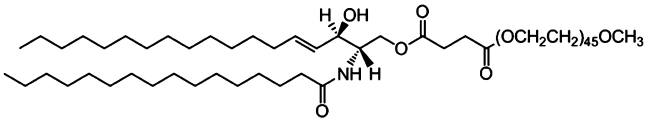

C16-PEG2000-Ceramide

EXPERIMENTAL SECTION

Materials and Sample Preparation. The DPPC, diC7PC, and the C16-PEG2000-Ceramide are all purchased from Avanti Polar Lipids, Inc., and used without further purification. DPPC has a zwitterionic hydrophilic head and long hydrocarbon tails, while the diC7PC has the same headgroup structure as the DPPC but it has much shorter hydrocarbon tails than DPPC. Using diC7PC as the short-chain species could avoid the free monomer concentration issue that occurs in studying the DMPC/DHPC (1,2-dihexanoyl-*sn*-glycero-3-phosphocholine) bicelle system.[40] diC7PC has a much lower critical micelle concentration than the DHPC in pure systems. A dilution experiment showed that the size of the diC7PC/DPPC bicelles remains unchanged upon dilution with pure water (Figure S1 in Supporting Information (SI)), which indicates that the amount of free diC7PC monomers in coexistence with the bicelles is negligible as compared with the total concentration of diC7PC in the sample of DPPC/diC7PC mixtures with typical lipid concentrations for preparing bicelles. The C16-PEG2000-Ceramide also has two long hydrocarbon tails similar to the DPPC. The DPPC and diC7PC are dissolved in chloroform separately, and C16-PEG2000-Ceramide is dissolved in the chloroform/methanol (9:1) mixture because of the large hydrophilic PEG group of the C16-PEG2000-Ceramide. The solutions are mixed with designated proportions. The sum of DPPC and C16-PEG2000-Ceramide concentrations is fixed at 10 mM, with the percentage of C16-PEG2000-Ceramide in this sum varied from 0 to 10%, 20%, and 30%. The short-chain lipid diC7PC concentration is fixed at 3.3 mM. The lipid solutions are dried in a hood overnight, followed by 8 h of drying under vacuum to completely remove the solvents. Finally, purified water is added, and the solutions are sonicated at 50 °C to ensure the complete dissolution of the lipids.

SAXS Measurements. The SAXS measurements were conducted at beam line 23A of the National Synchrotron Radiation Research Center (NSRRC), Hsinchu, Taiwan.[43] The X-ray energy was set at 15 keV, and the sample-to-detector distance (SDD) is about 3 m. The Q range covers from about 0.007 to 0.43 Å^{-1}. Here, the scattering vector Q is equal to $(4\pi/\lambda)\sin(\theta/2)$, where λ is the X-ray wavelength and θ is the scattering angle. The detector is a Pilatus 1M-F area detector with an effective size of 169 mm by 179 mm. The liquid samples were sealed in the sample cell with Kapton-walled windows, and the sample thickness is 2.5 mm. The samples were kept at 25 °C during the SAXS measurements using a thermostatically controlled circulation bath. The collected 2D data were circularly averaged to obtain the 1D scattering intensity distribution as a function of scattering vector. The measured scattering intensities were corrected for the detector sensitivity and background, and normalized to obtain the absolute scattering cross sections.

SAXS Data Analysis. Data analysis was carried out using the National Institute of Standards and Technology (NIST) Center for Neutron Research (NCNR) data analysis macros written for Igor Pro software.[44] In general, the scattering intensity $I(Q)$ can be expressed as

$$I(Q) = AQ^{-4} + P(Q)S(Q) + b \quad (1)$$

Here, A is the scale factor for the Porod term Q^{-4},[45,46] which accounts for the scattering contribution from large aggregates that coexist with dispersed bicelles. $P(Q)$ represents the form factor of the bicelle, which depends on the number density, size, shape, and structure of the bicelle. $S(Q)$ represents the interparticle structure factor.

In this study, the "PolyCoreBicelle" model of the NCNR package is used to calculate the form factor $P(Q)$.[44] This model assumes the bicelle core radius has a log-normal distribution. With the incorporation of PEGylated lipids in the bicelle, it is necessary to add one more hydrophilic shell to the bicelle model to account for the PEG brushes stretching out the headgroup layer. This two-shell disc bicelle model is illustrated in Figure 1. The hydrophilic headgroup shell layers on the rim and on the planar face may have different packing densities due to geometrical constraints,[5] and their X-ray scattering length densities will be different. Similarly, for the PEG brush layer, the scattering length density may be different for the rim

DOI: 10.1021/acs.langmuir.9b00756
Langmuir 2019, 35, 9483−9492

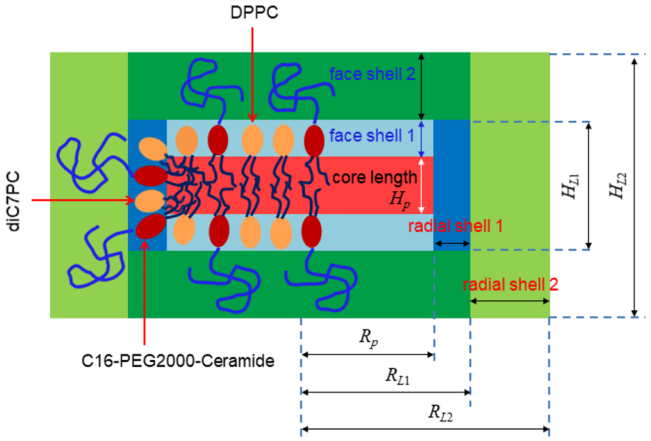

Figure 1. Illustration of the two-shell disc model (cut view) for fitting the SAXS profiles of DPPC/diC7PC/C16-PEG2000-Ceramide bicelles.

shell and the planar face layer since the distribution of the PEGylated lipids could be different in the rim and in the planar bilayer region. The disc-shaped bicelle form factor can be described by[44]

$$P(Q) = \frac{\text{scale}}{V_p}\sum_{R_p} n(R_p, \sigma_p)p(Q) \tag{2}$$

Here, "scale" is the amplitude term, and V_p is the particle volume. The log-normal distribution is given by

$$n(R_p, \sigma_p) = \frac{\exp\left(-\frac{1}{2}\left[\frac{\ln\left(\frac{R_p}{R_o}\right)}{\sigma_p}\right]^2\right)}{\sqrt{2\pi}\sigma_p R_p} \tag{3}$$

The original one-shell disc form factor used in "PolyCoreBicelle" model of the NCNR package is replaced with the two-shell disc form factor developed in this study and it is given by

$$\begin{aligned} p(Q) = \int_0^{\pi/2} \sin\theta\, d\theta \Bigg[& V_{p,p}(\rho_p - \rho_{f1})\frac{\sin\left(\frac{QH_p\cos\theta}{2}\right)}{\frac{QH_p\cos\theta}{2}}\frac{2J_1(QR_p\sin\theta)}{QR_p\sin\theta} \\ & + V_{p,L1}(\rho_{f1} - \rho_{r1})\frac{\sin\left(\frac{QH_{L1}\cos\theta}{2}\right)}{\frac{QH_{L1}\cos\theta}{2}}\frac{2J_1(QR_p\sin\theta)}{QR_p\sin\theta} \\ & + V_{L1,L1}(\rho_{r1} - \rho_{f2})\frac{\sin\left(\frac{QH_{L1}\cos\theta}{2}\right)}{\frac{QH_{L1}\cos\theta}{2}}\frac{2J_1(QR_{L1}\sin\theta)}{QR_{L1}\sin\theta} \\ & + V_{L1,L2}(\rho_{f2} - \rho_{r2})\frac{\sin\left(\frac{QH_{L2}\cos\theta}{2}\right)}{\frac{QH_{L2}\cos\theta}{2}}\frac{2J_1(QR_{L1}\sin\theta)}{QR_{L1}\sin\theta} \\ & + V_{L2,L2}(\rho_{r2} - \rho_{solv})\frac{\sin\left(\frac{QH_{L2}\cos\theta}{2}\right)}{\frac{QH_{L2}\cos\theta}{2}}\frac{2J_1(QR_{L2}\sin\theta)}{QR_{L2}\sin\theta}\Bigg]^2 \end{aligned} \tag{4}$$

with

$$V_{x,y} = \pi R_x^2 H_y \tag{5}$$

In the above equations, $J_1(x)$ is the first order Bessel function. R_p is the core radius (the mean core radius is R_o), and H_p is the core length (core height). R_{L1} is the core radius plus first shell thickness, and H_{L1} is the core length plus twice the first face shell thickness. R_{L2} and H_{L2} are the total radius and the total length (height), respectively. Sigma (σ_p) is equivalent to the standard deviation of the log-normal distribution. The scattering length density (SLD) of the core, the first rim shell, the second rim shell, the first face shell, the second face shell, and the solvent are expressed as ρ_p, ρ_{r1}, ρ_{r2}, ρ_{f1}, ρ_{f2}, and ρ_{solv}, respectively. The hard sphere structure model of the NCNR package is used to model the interparticle structure factor $S(Q)$.[44] The hard sphere structure factor $S(Q)$ depends on the following parameters: the effective particle diameter and the volume fraction of the particle in the solution.[44,47,48] For fitting the SAXS profiles from multilayer particle systems, the scattering contrast of each layer would affect the shape of the scattering profile as well as the scattering amplitude, the "scale" parameter. Both the amplitude parameter and the scattering contrasts can be set as free fitting parameters. Usually, the scattering contrast of the core is well-defined, and its value can be constrained to be close to the theoretical value during the fitting process.

RESULTS AND DISCUSSION

The measured SAXS profiles of DPPC/diC7PC/C16-PEG2000-Ceramide bicelles together with the fitted curves are shown in Figure 2. The total DPPC and C16-PEG2000-Ceramide concentration is kept at a constant of 10 mM, and the percentage of C16-PEG2000-Ceramide is increased from 0 to 10, to 20, to 30 mol %, values which correspond to the added C16-PEG2000-Ceramide concentrations of 0, 1, 2 and 3 mM, respectively. The diC7PC is fixed at 3.3 mM for all four

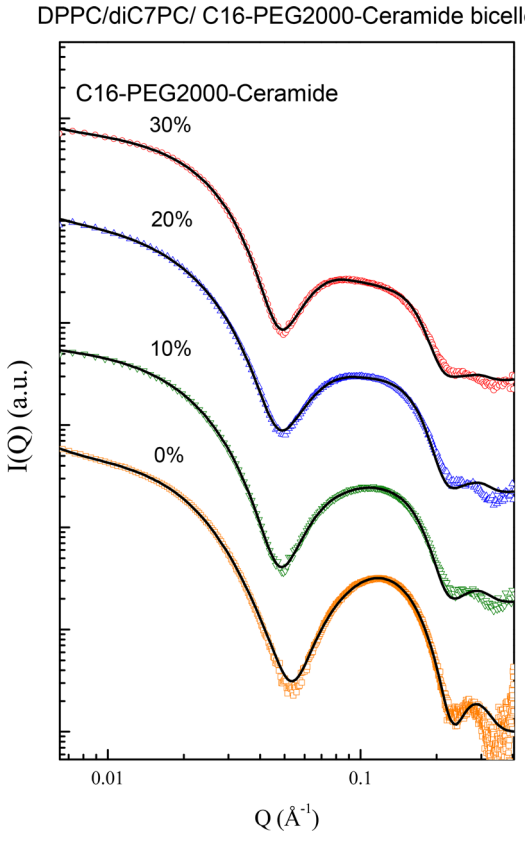

Figure 2. SAXS profiles of DPPC/diC7PC/C16-PEG2000-Ceramide bicelles. The percentage of the C16-PEG2000-Ceramide of the total long-chain lipids is increased from 0, to 10%, to 20%, and to 30%, which correspond to 0, 1, 2, and 3 mM C16-PEG2000-Ceramide, respectively. The total concentration of the long-chain lipids, including the DPPC and the C16-PEG2000-Ceramide, is kept at 10 mM. The concentration of diC7PC is kept at 3.3 mM. The scattering curves are shifted for clarity.

DOI: 10.1021/acs.langmuir.9b00756
Langmuir 2019, 35, 9483−9492

Table 1. Fitting Parameters for the SAXS Profiles of Bicelles Incorporated with Different Amounts of C16-PEG2000-Ceramide[a]

	DPPC/diC7PC bicelle	10% C16-PEG2000-Ceramide bicelle	20% C16-PEG2000-Ceramide bicelle	30% C16-PEG2000-Ceramide bicelle
A (the scale factor of the Q^{-4})	$1.9 \times 10^{-10} \pm 10\%$	$3.0 \times 10^{-11} \pm 10\%$	$2.1 \times 10^{-10} \pm 10\%$	$1.3 \times 10^{-10} \pm 10\%$
		$P(Q)$		
scale	0.0224 ± 3%	0.0723 ± 3%	0.102 ± 3%	0.102 ± 3%
mean core radius (Å)	99.5 ± 5.0	81.1 ± 3.0	66.0 ± 3.0	50.5 ± 3.0
radial polydispersity	0.20 ± 0.02	0.33 ± 0.02	0.39 ± 0.02	0.41 ± 0.02
core length (Å)	25.5 ± 0.3	25.5 ± 0.3	25.5 ± 0.3	25.5 ± 0.3
radial shell 1 thickness (Å)	15.3 ± 1.0	15.3 ± 1.0	15.3 ± 1.0	15.3 ± 1.0
radial shell 2 thickness (Å)		35.0 ± 3.0	35.0 ± 3.0	35 ± 3.0
face shell 1 thickness (Å)	15.5 ± 0.4	16.0 ± 0.5	16.5 ± 0.5	17.3 ± 0.5
face shell 2 thickness (Å)		35.0 ± 2.0	35.0 ± 2.0	35.0 ± 2.0
SLD core ($\times 10^{-6}$ Å^{-2})	8.32 ± 0.03	8.32 ± 0.03	8.32 ± 0.03	8.32 ± 0.03
SLD face 1 ($\times 10^{-6}$ Å^{-2})	10.96 ± 0.02	10.86 ± 0.03	10.73 ± 0.03	10.71 ± 0.06
SLD face 2 ($\times 10^{-6}$ Å^{-2})		9.491 ± 0.01	9.528 ± 0.01	9.569 ± 0.01
SLD rim 1 ($\times 10^{-6}$ Å^{-2})	9.55 ± 0.03	9.60 ± 0.02	9.83 ± 0.03	9.71 ± 0.05
SLD rim 2 ($\times 10^{-6}$ Å^{-2})		9.438 ± 0.01	9.468 ± 0.01	9.470 ± 0.02
SLD solvent ($\times 10^{-6}$ Å^{-2})	9.41	9.41	9.41	9.41
		$S(Q)$		
hard sphere diameter (Å)	164 ± 30	170 ± 15	150 ± 15	165 ± 15
volume fraction	0.017 ± 0.03	0.060 ± 0.01	0.060 ± 0.01	0.060 ± 0.01
b (background) (cm^{-1})	0.00096 ± 5%	0.0018 ± 5%	0.0062 ± 5%	0.0027 ± 5%

[a]The percentage of the C16-PEG2000-Ceramide of the total long-chain lipids is increased from 0, to 10%, to 20%, to 30%, which correspond to 0, 1, 2, and 3 mM C16-PEG2000-Ceramide, respectively. The total concentration of DPPC and C16-PEG2000-Ceramide is fixed at 10 mM. The concentration of diC7PC is kept at 3.3 mM.

samples. The SAXS profiles of these four mixed lipid samples exhibit the typical feature of disc-shaped bicelles with a pronounced first interference fringe. The hydrocarbon core of the bicelle has an X-ray SLD slightly lower than the SLD of water, and the headgroup layer has a higher SLD than the SLD of water. For X-ray scattering, the bicelle somewhat resembles a shell-like object. Scattering from a shell-like structure would result in a pronounced first interference fringe. As shown in Figure 2, the first interference fringe changes gradually from a smooth round shape to become a flat top shape as the concentration of the added C16-PEG2000-Ceramide is increased from 0 to 1, to 2, to 3 mM. It is noticeable that a bump grows at around $Q = 0.075$ Å^{-1} as the C16-PEG2000-Ceramide concentration is increased. It is evident that the change of the first interference fringe is due to the presence of the incorporated C16-PEG2000-Ceramide lipids. The shell structure of the bicelle has been changed to a structure that is more complex than just a single layer structure due to the incorporation of C16-PEG2000-Ceramide lipids. It is expected that the 45 hydrophilic oxyethylene segments of C16-PEG2000-Ceramide would stretch out to form a brush layer as depicted in the fitting model of Figure 1. In addition to the lipid headgroup shell, there will be a brush layer outside the headgroup layer. A two-shell disc-shaped bicelle model is needed for analyzing the SAXS profiles of the DPPC/diC7PC/C16-PEG2000-Ceramide bicelles. The two-shell bicelle model is described in the SAXS Data Analysis section. As shown in Figure 2, all the measured SAXS profiles are well-fit by this two-shell disc bicelle model. The fitting parameters are listed in Table 1. The contribution of the Porod term Q^{-4} is very small, which indicates that the amounts of the nondispersed lipids are very small. The respective contributions of the form factors $P(Q)$ and $S(Q)$ to the SAXS profiles are shown in Figure 3a–d for the cases with 0, 1, 2, and 3 mM C16-PEG2000-Ceramide added. The interparticle structure factor $S(Q)$ mainly affects the low Q region. Although there is no charge interaction between the bicelles and the lipid concentration is also relatively dilute, the excluded volume effect still exists. The scattering intensity and the profile in the low Q region are slightly modified by the $S(Q)$ term as shown in Figure 3. The obtained volume fraction parameter of the hard sphere $S(Q)$ model is listed in Table 1. The volume fraction parameter increases from 0.017 for the DPPC/diC7PC bicelle case to around 0.060 for the cases with C16-PEG2000-Ceramide added. Since the bicelles incorporated with C16-PEG2000-Ceramide possess the additional PEG brush shell, it is expected that the excluded volume effect would be greater for the cases with C16-PEG2000-Ceramide incorporated.

As for the bicelle structure, the hydrophobic core height is found to be around 25.5 Å, and the thickness of radial shell 1 is about 15.3 Å for all cases, while the thickness of the face 1 shell increases slightly from 15.5 to 17.3 Å as the C16-PEG2000-Ceramide concentration is increased from 0 to 3 mM. It seems that the packing of the headgroups is slightly affected when incorporating some C16-PEG2000-Ceramide lipids in the planar region. The SLD of the face 1 shell decreases slightly from 10.96×10^{-6} to 10.71×10^{-6} Å^{-2}. Such SLD values are typical for the headgroup layer of the lipid bilayer. The SLD of the rim 1 shell varied between 9.55×10^{-6} and 9.83×10^{-6} Å^{-2}, which is lower than the value of the face 1 shell. This is due to the packing of the headgroups in the rim shell being less dense than that in the planar bilayer region. The lipids in the planar bilayer region have better ordering than the lipids in the rim shell. The SLD of the bicelle hydrocarbon core is found to be around 8.32×10^{-6} Å^{-2}, which is slightly lower than the SLD of water as mentioned earlier. It is also important to determine the bicelle core radius since it is related to how the added C16-PEG2000-Ceramide lipids are distributed in the

DOI: 10.1021/acs.langmuir.9b00756
Langmuir 2019, 35, 9483–9492

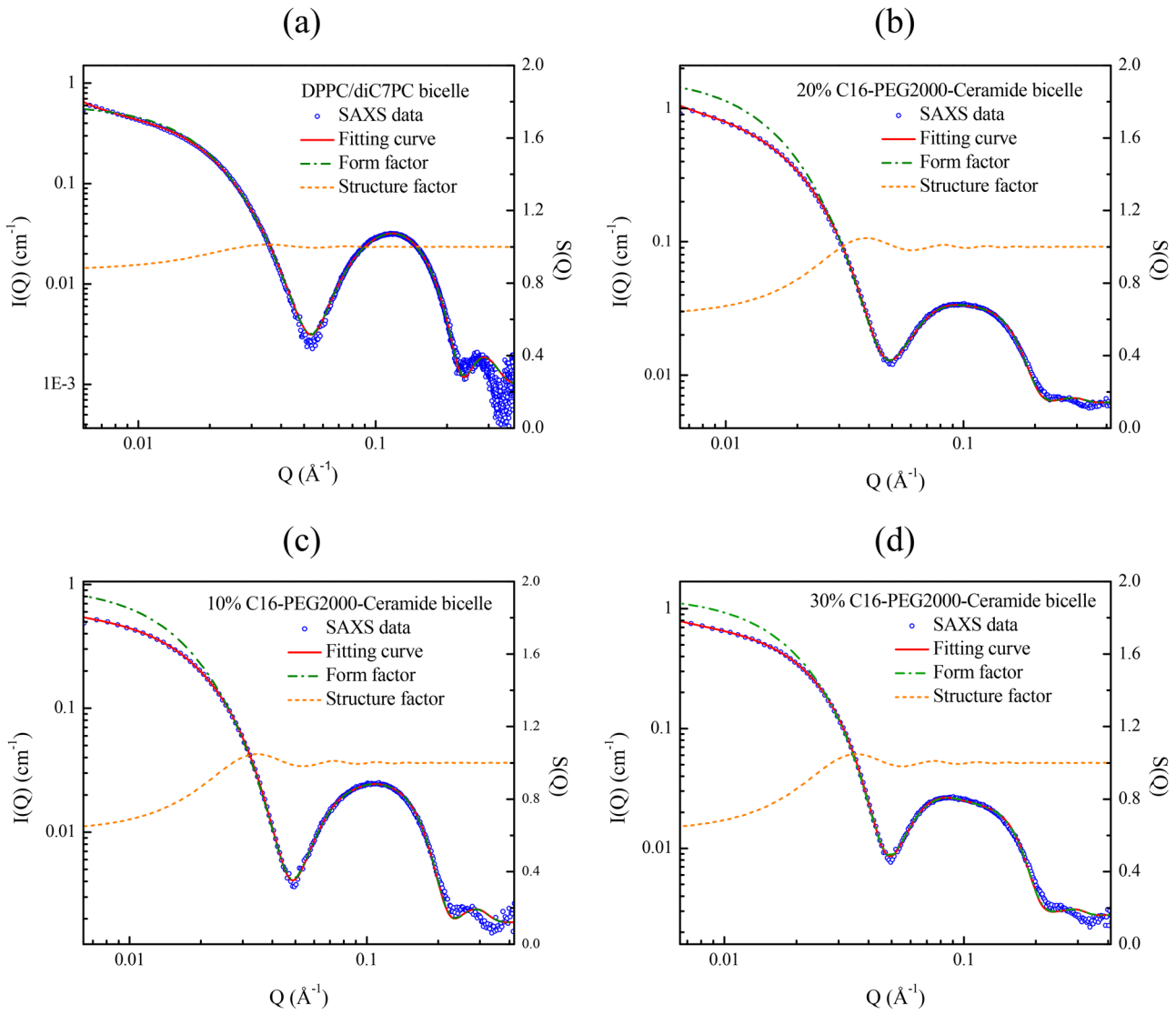

Figure 3. SAXS fitting profiles including form factor and structure factor: (a) DPPC/diC7PC bicelles, (b) 10% C16-PEG2000-Ceramide bicelle, (c) 20% C16-PEG2000-Ceramide bicelle, and (d) 30% C16-PEG2000-Ceramide bicelle.

bicelle. The bicelle core radius is found to decrease from 99.5 to 81.1, to 66.0, and to 50.5 Å, respectively, for the C16-PEG2000-Ceramide concentrations of 0, 1, 2, and 3 mM cases. The shrinking in core radius means that some of the added C16-PEG2000-Ceramide lipids are incorporated in the rim. If all the added C16-PEG2000-Ceramide lipids lie in the planar region, the bicelle size should remain about the same since the total DPPC and C16-PEG2000-Ceramide concentration is fixed.

In this study, it is most important to determine the size and SLD of the PEG brush shells in the planar region and in the rim of the bicelle incorporated with C16-PEG2000-Ceramide lipids. The profile of the first interference fringe is mainly affected by the brush layer thickness and SLD of the planar region (face 2 layer), while the brush layer thickness and SLD of the rim shell mainly affect the SAXS profile in the region $Q < 0.05$ Å^{-1}. Thus, it is possible to separate the scattering contributions from the planar region and the rim. The thickness of the PEG brush layer is found to be around 35 Å both in the planar region and in the rim with an uncertainty of ~2−3 Å. This value agrees with the value of 35 Å of the PEG shell thickness obtained by the dynamic light scattering study of a spherical PEG(2000)-DSPE (1,2-distearoyl-*sn*-glycero-3-phosphoethanolamine-*N*-[methoxy(polyethylene glycol)-2000]) micelle, and it is also very close to the theoretical estimated layer thickness of 34 Å.[49] The SLD of the face 2 shell (the PEG brush layer in the planar region) is found to increase from 9.491×10^{-6} to 9.528×10^{-6} and to 9.569×10^{-6} Å^{-2}, respectively, for the 1, 2, and 3 mM C16-PEG2000-Ceramide cases. For the SLD of the rim 2 shell (the PEG brush shell in the rim), it is found to increase from 9.438×10^{-6} to 9.468×10^{-6} and to 9.470×10^{-6} Å^{-2}, respectively, for the 1, 2, and 3 mM C16-PEG2000-Ceramide cases. These SLD values are higher than the SLD value of water, 9.41×10^{-6} Å^{-2}, which indicates the presence of PEG brushes both in the face 2 shell and the rim 2 shell. It is evident that the C16-PEG2000-Ceramide lipids are distributed both in the planar region as well as in the rim of the bicelle. The numbers of the C16-PEG2000-Ceramide lipids in the planar region and in the rim can be calculated from these SLD values and the shell volumes. The SLD of PEG2000 used in the calculation is estimated to be 11.1×10^{-6} Å^{-2}. As listed in Table 2, the number of the C16-PEG2000-Ceramide lipids in the planar region varies from 35.1 to 36.4 and to 32.1 as the concentration of C16-

DOI: 10.1021/acs.langmuir.9b00756
Langmuir 2019, 35, 9483−9492

Table 2. Lipid Numbers of Each Lipid Species per Bicelle[a]

	10% PEGlated lipid bicelle	20% PEGlated lipid bicelle	30% PEGlated lipid bicelle
total number of lipids per bicelle	711	471	276
expected DPPC lipid number per bicelle	480	282	145
expected diC7PC lipid number per bicelle	178	118	69
expected total C16-PEG2000-Ceramide lipid number per bicelle	53	71	62
C16-PEG2000-Ceramide Lipids in the Planar Region			
number per bicelle	35.1 ± 3.0	36.4 ± 3.0	32.1 ± 2.0
mol % in the planar region (%)	6.8 ± 0.6	11.4 ± 0.9	18.1 ± 1.1
C16-PEG2000-Ceramide Lipids in the Rim			
number per bicelle	19.0 ± 5.0	34.4 ± 5.0	30.4 ± 5.0
mol % in the rim (%)	9.6 ± 2.5	22.6 ± 3.3	30.6 ± 5.0
total C16-PEG2000-Ceramide lipids per bicelle by SAXS analysis	54.1 ± 5.8	70.8 ± 5.8	62.5 ± 5.4
q_a	2.62	2.10	1.78

[a]The total number of lipids per bicelle is estimated from the hydrophobic core volume obtained from the SAXS analysis. The expected numbers of DPPC, diC7PC, and C16-PEG2000-Ceramide lipids per bicelle are calculated according to their concentration ratios in the solution. The numbers of C16-PEG2000-Ceramide lipid in the planar region and in the rim are calculated from the SLD values in the face 2 and rim 2 regions. All the DPPC is assumed to lie in the planar region, and all the diC7PC is assumed to lie in the rim when calculating the mol % of the C16-PEG2000-Ceramide in the planar region and in the rim. Here q_a is defined as the ratio of the lipid number in the planar region to the lipid number in the rim.

PEG2000-Ceramide is increased from 1 to 2 and to 3 mM, respectively. In the meantime, the number of the C16-PEG2000-Ceramide lipids in the rim varies from 19.0 to 34.4 and to 30.4 as the concentration of C16-PEG2000-Ceramide is increased from 1 to 2 and to 3 mM, respectively. For the 1 mM C16-PEG2000-Ceramide case, only about 35% C16-PEG2000-Ceramide lipids lie in the rim. As the C16-PEG2000-Ceramide concentration is increased to 2 and 3 mM and the DPPC concentration is reduced to 8 and 7 mM, respectively, about half of the C16-PEG2000-Ceramide lipids lie in the rim. It is evident that the added C16-PEG2000-Ceramide lipids are distributed both in the planar region as well as in the rim of the bicelle.

Instead of looking at the lipid numbers of the distributed C16-PEG2000-Ceramide lipids, it is more meaningful to discuss the lipid percentages of C16-PEG2000-Ceramide in the planar region and also in the rim since the lipid number in the planar region and in the rim vary with the added C16-PEG2000-Ceramide concentration due to the changes in bicelle size. To calculate the C16-PEG2000-Ceramide lipid percentages, one would need to know the lipid number of DPPC and diC7PC per bicelle. The total number of lipids in one bicelle can be estimated from the constraint of the total hydrocarbon tail volume in the bicelle by

$$N_t = \pi R_0^2 H_p / [(q_0 V_L + V_S)/(q_0 + 1)] \quad (6)$$

Since the C16-PEG2000-Ceramide has hydrocarbon tails similar to the DPPC, its tail volume is assumed to be the same as the DPPC of V_L. The hydrocarbon tail volume of diC7PC is denoted as V_S. The hydrocarbon tail volumes V_L and V_S are estimated as 862 and 378 Å^3, respectively.[50] Here, q_0 denotes the molar ratio of the total long-chain lipid to the short-chain lipid in the solution as given by

$$q_0 = \frac{[\text{DPPC}] + [\text{PEGlipid}]}{[\text{diC7PC}]} = \frac{N_{\text{DPPC}} + N_{\text{PEGlipid}}}{N_{\text{diC7PC}}} \quad (7)$$

In this study q_0 is fixed at 3. As shown in eq 7, the ratio of the total lipid number of DPPC lipid (N_{DPPC}) and C16-PEG2000-Ceramide lipid (N_{PEGlipid}) in one bicelle to the diC7PC lipid number (N_{diC7PC}) in one bicelle is assumed also to be equal to q_0. The number of the diC7PC lipid in one bicelle can be calculated from N_t using $N_{\text{diC7PC}} = N_t/(q_0 + 1)$. The total number of DPPC and C16-PEG2000-Ceramide lipids in one bicelle is given by $N_{\text{DPPC}} + N_{\text{PEGlipid}} = N_t(q_0/(q_0 + 1))$. The expected number of C16-PEG2000-Ceramide lipid N_{PEGlipid} per bicelle can be obtained from the added percentage of C16-PEG2000-Ceramide of the total long-chain lipids. For example, for the 10 mol % C16-PEG2000-Ceramide case, the expected total number of C16-PEG2000-Ceramide lipids per bicelle is given by $N_{\text{PEGlipid}} = 0.1N_t(q_0/(q_0 + 1))$. The calculated lipid numbers of the three lipid species for the samples containing C16-PEG2000-Ceramide are listed in Table 2. It is now possible to calculate the percentages of the C16-PEG2000-Ceramide lipid in the planar region as well as in the rim by assuming that all the DPPC lipids lie in the planar region and all the diC7PC lipids lie in the rim. As listed in Table 2, the C16-PEG2000-Ceramide lipid percentage in the planar region increases from 6.8 to 11.4 and to 18.1 mol % when the C16-PEG2000-Ceramide concentration is increased from 1 to 2 and to 3 mM, respectively. In the bicelle rim, the C16-PEG2000-Ceramide lipid percentage increases from 9.6 to 22.6 and to 30.6 mol % when the C16-PEG2000-Ceramide concentration is increased from 1 to 2 and to 3 mM, respectively. Figure 4 shows the dependence of the C16-PEG2000-Ceramide lipid percentages in the planar region and

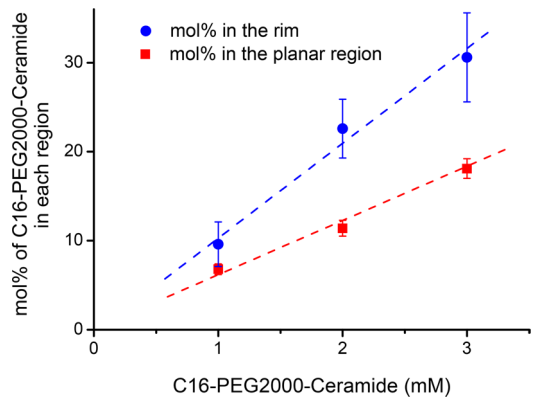

Figure 4. Mol % of C16-PEG2000-Ceramide lipids in the planar region and in the rim of the bicelle as a function of the C16-PEG2000-Ceramide concentration. The total concentration of DPPC and C16-PEG2000-Ceramide is kept at a constant of 10 mM, while the diC7PC is kept at 3.3 mM. The mol % in the planar region is calculated by dividing the number of C16-PEG2000-Ceramide species in the planar region by the number sum of the DPPC and the C16-PEG2000-Ceramide in the planar region. The mol % in the rim is calculated by dividing the number of C16-PEG2000-Ceramide species in the rim by the number sum of the diC7PC and the C16-PEG2000-Ceramide species in the rim. The dashed lines are used to indicate the trend of the dependence on the C16-PEG2000-Ceramide concentration.

DOI: 10.1021/acs.langmuir.9b00756
Langmuir 2019, 35, 9483−9492

in the rim as a function of C16-PEG2000-Ceramide concentration. Both the C16-PEG2000-Ceramide lipid densities in the planar region and in the rim tend to increase linearly with increasing C16-PEG2000-Ceramide concentration. The lipid density of C16-PEG2000-Ceramide in the rim is about 1.7 times the C16-PEG2000-Ceramide lipid density in the planar region for these three C16-PEG2000-Ceramide concentrations. For the 3 mM C16-PEG2000-Ceramide case, about one-third of the lipids in the rim are C16-PEG2000-Ceramide, while only about one-fifth of the lipids in the planar region are C16-PEG2000-Ceramide. The higher C16-PEG2000-Ceramide lipid density in the rim than in the planar region might be related to the difference in the available interface area per lipid in the rim and in the planar region. The interface area per diC7PC in the rim is estimated about 1.7 times the interface area of DPPC in the planar region.[51] This means that the total interface area of three lipids in the rim is roughly equal to the total interface area of five lipids in the planar region. This may explain why there is one C16-PEG2000-Ceramide lipid per three lipids in the rim and only one C16-PEG2000-Ceramide lipid per five lipids in the planar region for the 3 mM C16-PEG2000-Ceramide case. It is likely that the C16-PEG2000-Ceramide lipid density difference in the planar region and in the rim is due to every C16-PEG2000-Ceramide preferring to occupy approximately the same interface area size regardless of being in the planar region or in the rim in order to accommodate its bulky PEG brush. The sum of the C16-PEG2000-Ceramide lipid numbers in the planar region and in the rim as determined from the SAXS analysis is also listed in Table 2. This SAXS determined total C16-PEG2000-Ceramide lipid number in one bicelle is supposed to be the same as that derived from the volume constraint, eq 6. As listed in Table 2, for all three C16-PEG2000-Ceramide concentration cases, the total C16-PEG2000-Ceramide lipid numbers per bicelle as determined by SAXS analysis agree very well with the expected total numbers of C16-PEG2000-Ceramide lipid per bicelle derived from the volume constraint equation. This is a useful way to check the consistency of the SAXS fitting.

Since the added C16-PEG2000-Ceramide lipids are distributed both in the rim as well as in the planar region, the ratio of the lipid number in the planar region to the lipid number in the rim will vary according to the actual lipid distribution. This actual lipid ratio is defined as q_a:

$$q_a = \frac{N_{DPPC} + N_{PEGlipid,P}}{N_{diC7PC} + N_{PEGlipid,R}} \quad (8)$$

Here, $N_{PEGlipid,P}$ is the C16-PEG2000-Ceramide lipid number in the planar region and $N_{PEGlipid,R}$ is the C16-PEG2000-Ceramide lipid number in the rim. This lipid ratio q_a decreases from 3.0 to 2.62, to 2.10, and to 1.78, as the concentration of the C16-PEG2000-Ceramide is increased from 0 to 1, to 2, and to 3 mM, respectively. Theoretically, the bicelle size is tightly related to the parameter q_a. As shown in Figure 5, the bicelle core radius is found to decrease with decreasing q_a. The bicelle size will shrink if there are more lipids available for covering the rim, or when the lipid number for the planar region is reduced. Theoretically, it is possible to relate the bicelle size to the lipid ratio parameter q_a on the basis of the geometrical packing consideration of the volume constraint.[52,53] Instead of the parameter q_0, the actual lipid ratio q_a should be used in the bicelle size model calculation since the parameter q_0 does not

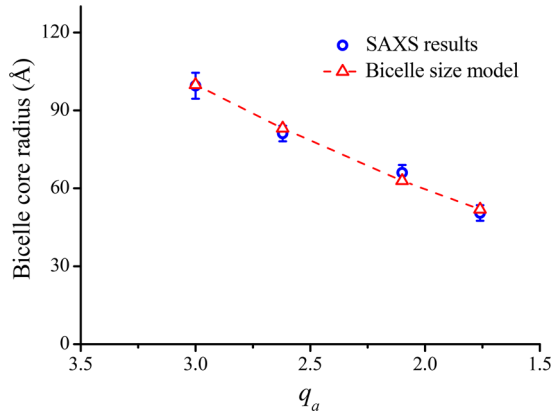

Figure 5. Bicelle core radius as a function of the parameter q_a, which is the ratio of the lipid number in the planar region to the lipid number in the rim. Upon addition of the C16-PEG2000-Ceramide lipids, some of the C16-PEG2000-Ceramide lipids are incorporated in the rim, and some of the C16-PEG2000-Ceramide lipids are incorporated in the planar region. The parameter q_a is changed due to the addition of C16-PEG2000-Ceramide lipids. Here, the parameter q_a is defined as the total lipid number in the planar region, including all DPPC lipids and the C16-PEG2000-Ceramide lipids in the planar region, divided by the total lipid number in the rim, including all the diC7PC lipids and the C16-PEG2000-Ceramide lipids in the rim. In this study, the total concentration of DPPC and C16-PEG2000-Ceramide is kept at a constant of 10 mM, while the diC7PC is kept at 3.3 mM. The q_a parameter decreases from 3.0 to 2.62, to 2.10, and to 1.78, respectively, for the 0, 1, 2, and 3 mM C16-PEG2000-Ceramide cases. The bicelle size model is calculated according to eq 9.

take into account the distribution of C16-PEG2000-Ceramide lipids in the rim. Using the actual lipid ratio q_a and the modified lipid volume ratio parameter λ^*, a slightly modified bicelle size model is given by[52]

$$R_0 = \frac{r_\perp q_a}{4\lambda^*}\left(\pi + \sqrt{\pi^2 + \frac{32\lambda^*}{3q_a}}\right) \quad (9)$$

Here $r_\perp$ is the length of the short-chain lipid molecule. For the short-chain lipid DHPC, a length of 11 Å is used for $r_\perp$.[52,53] As for the diC7PC used in this study, a value of 12.3 Å is used for $r_\perp$ since the diC7PC has a tail length about 1.3 Å longer than the DHPC tail length and the headgroup of the diC7PC is the same as that of DHPC. In eq 9, the modified parameter λ^* is used to replace the original parameter λ.[52,53] This bicelle size model was originally developed for evaluating the size of the DMPC/DHPC bicelles. Here, DMPC is the long-chain lipid 1,2-dimyristoyl-*sn*-glycero-3-phosphocholine. The parameter λ is defined as the molecular volume ratio of the lipids in the rim to the lipids in the planar region. For the DMPC/DHPC bicelles, the parameter λ is equal to the molecular volume ratio of DHPC to DMPC with the assumption that all the DMPC species lie in the planar region and DHPC lies in the rim.[52,53] In this study, it is necessary to modify this parameter λ by taking into account the presence of C16-PEG2000-Ceramide lipids in the rim. The modified parameter λ^* is defined as the averaged lipid molecular volume in the rim to the averaged lipid molecular volume in the planar region but excluding the brush volume of the C16-PEG2000-Ceramide. This modified lipid volume ratio parameter is given by

$$\lambda^* = \lambda(1 - \alpha) + \alpha \quad (10)$$

DOI: 10.1021/acs.langmuir.9b00756
Langmuir 2019, 35, 9483−9492

Here, α is the mol % of the C16-PEG2000-Ceramide lipid in the rim. It is approximated that the head plus tail volume of the C16-PEG2000-Ceramide is the same the head plus tail volume of DPPC. Unlike the constant parameter λ, the parameter λ^* varies with the concentration of the C16-PEG2000-Ceramide. In this study, the parameter λ in eq 10 is the molecular volume ratio of diC7PC to DPPC, which is estimated to be 0.61. Equation 9 can be used to estimate the bicelle core radius of the DPPC/diC7PC/C16-PEG2000-Ceramide bicelles by using the actual lipid ratio q_a and the modified lipid volume ratio λ^*. The bicelle core radius calculated according to this modified model together with the bicelle core radius determined by SAXS fitting is plotted in Figure 5. As shown in Figure 5, the theoretically predicted core radius agrees quite well with the experimentally determined core radius. It seems that the bicelle core size can be well-predicted by such a volume constraint model if correct lipid ratio q_a and the modified lipid volume ratio λ^* are used in the calculation.

CONCLUSIONS

In this study, SAXS successfully reveals the structure of the DPPC/diC7PC bicelles incorporated with different amounts of C16-PEG2000-Ceramide lipids. Due to the high X-ray contrast of the headgroup and brush shells of the disc-shaped bicelles, it is possible to determine the distribution of the added C16-PEG2000-Ceramide lipids. It may not be surprising that the C16-PEG2000-Ceramide lipids could distribute surrounding the curved rim, similar to the short-chain lipids with a spontaneous positive curvature.[49] Contrary to the popular belief, a good portion of the added C16-PEG2000-Ceramide lipids are found to lie in the planar region of the bicelle only with a lower lipid number density as compared with that in the rim (Figure 6). This finding is important for preparing bicelles incorporated with PEGylated lipids for enhancing the antifouling properties. It is also important to know that the lipid densities of C16-PEG2000-Ceramide both in the planar region and in the rim increase approximately linearly in proportion to the C16-PEG2000-Ceramide concentration. The dependence of the bicelle core radius on the actual ratio of the lipids in the planar region to the lipids in the rim can be well-predicted based on the volume constraint model.

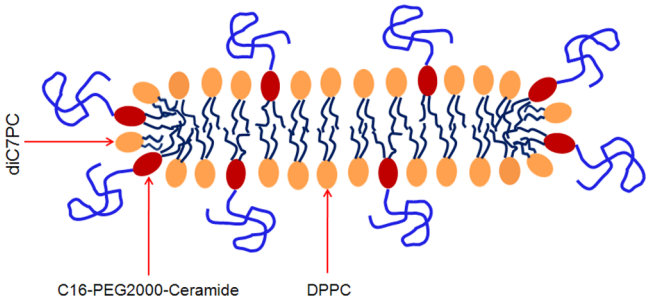

Figure 6. Schematic cut view of the disc-shaped bicelle incorporated with C16-PEG2000-Ceramide lipids. The incorporated C16-PEG2000-Ceramide lipids are distributed not just in the rim of the bicelle but also in the planar bilayer region.

ASSOCIATED CONTENT

Supporting Information

The Supporting Information is available free of charge on the ACS Publications website at DOI: 10.1021/acs.langmuir.9b00756.

SAXS dilution experiment of the DPPC/diC7PC system (PDF)

AUTHOR INFORMATION

Corresponding Author

*Phone: +886-3-5742671. Fax: 886-3-5728445. E-mail: tllin@mx.nthu.edu.tw.

ORCID

Tsang-Lang Lin: 0000-0001-7638-2066

U-Ser Jeng: 0000-0002-2247-5061

Notes

The authors declare no competing financial interest.

ACKNOWLEDGMENTS

We would like to thank the National Synchrotron Radiation Research Center (NSRRC) for providing the SAXS beam time and help with the measurements. This research is supported by the Ministry of Science and Technology, Taiwan, ROC, project nos. MOST 106-2113-M-007-019 (T.-L.L.) and MOST 107-2113-M-007-007 (T.-L.L.).

REFERENCES

(1) Lin, T.-L.; Liu, C.-C.; Roberts, M. F.; Chen, S.-H. Structure of Mixed Short-Chain Lecithin/Long-Chain Lecithin Aggregates Studied by Small-Angle Neutron Scattering. *J. Phys. Chem.* **1991**, *95*, 6020−6027.

(2) Gabriel, N. E.; Roberts, M. F. Interaction of Short-Chain Lecithin with Long-Chain Phospholipids: Characterization of Vesicles That Form Spontaneously. *Biochemistry* **1986**, *25*, 2812−2821.

(3) Eum, K. M.; Riedy, G.; Langley, K. H.; Roberts, M. F. Temperature-Induced Fusion of Small Unilamellar Vesicles Formed from Saturated Long-Chain Lecithins and Diheptanoylphosphatidylcholine. *Biochemistry* **1989**, *28*, 8206−8213.

(4) Bian, J.; Roberts, M. F. Phase Separation in Short-Chain Lecithin/Gel-State Long-Chain Lecithin Aggregates. *Biochemistry* **1990**, *29*, 7928−7935.

(5) Yang, P.-W.; Lin, T.-L.; Hu, Y.; Jeng, U-S. Small-Angle X-ray Scattering Studies on the Structure of Mixed DPPC/diC$_7$PC Micelles in Aqueous Solutions. *Chin. J. Phys.* **2012**, *50*, 349−356.

(6) Hu, A.; Fan, T.-H.; Katsaras, J.; Xia, Y.; Li, M.; Nieh, M.-P. Lipid-based nanodiscs as models for studying mesoscale coalescence − a transport limited case. *Soft Matter* **2014**, *10*, 5055−5060.

(7) Kučerka, N.; Nagle, J. F.; Sachs, J. N.; Feller, S. E.; Pencer, J.; Jackson, A.; Katsaras, J. Lipid Bilayer Structure Determined by the Simultaneous Analysis of Neutron and X-Ray Scattering Data. *Biophys. J.* **2008**, *95*, 2356−2367.

(8) Li, J.; Wang, X.; Zhang, T.; Wang, C.; Huang, Z.; Luo, X.; Deng, Y. A review on phospholipids and their main applications in drug delivery systems. *Asian J. Pharm. Sci.* **2015**, *10*, 81−98.

(9) Lin, T.-L.; Chen, S.-H.; Gabriel, N. E.; Roberts, M. F. Use of Small-Angle Neutron Scattering to Determine the Structure and Interaction of Dihexanoylphosphatidylcholine Micelles. *J. Am. Chem. Soc.* **1986**, *108*, 3499−3507.

(10) Lin, T.-L.; Chen, S.-H.; Gabriel, N. E.; Roberts, M. F. Small-Angle Neutron Scattering Techniques Applied to the Study of Polydisperse Rodlike Diheptanoylphosphatidylcholine Micelles. *J. Phys. Chem.* **1987**, *91*, 406−413.

(11) Luchette, P. A.; Vetman, T. N.; Prosser, R. S.; Hancock, R. E. W.; Nieh, M.-P.; Glinka, C. J.; Krueger, S.; Katsaras, J. Morphology of

DOI: 10.1021/acs.langmuir.9b00756
Langmuir 2019, 35, 9483−9492

fast-tumbling bicelles: a small angle neutron scattering and NMR study. *Biochim. Biophys. Acta, Biomembr.* **2001**, *1513*, 83−94.
(12) Warschawski, D. E.; Arnold, A. A.; Beaugrand, M.; Gravel, A.; Chartrand, É.; Marcotte, I. Choosing membrane mimetics for NMR structural studies of transmembrane proteins. *Biochim. Biophys. Acta, Biomembr.* **2011**, *1808*, 1957−1974.
(13) Katsaras, J.; Harroun, T. A.; Pencer, J.; Nieh, M.-P. "Bicellar" Lipid Mixtures as used in Biochemical and Biophysical Studies. *Naturwissenschaften* **2005**, *92*, 355−366.
(14) Ujwal, R.; Bowie, J. U. Crystallizing membrane proteins using lipidic bicelles. *Methods* **2011**, *55*, 337−341.
(15) Marcotte, I.; Auger, M. Bicelles as Model Membranes for Solid- and Solution-State NMR Studies of Membrane Peptides and Proteins. *Concepts Magn. Reson., Part A* **2005**, *24A*, 17−37.
(16) Piai, A.; Fu, Q.; Dev, J.; Chou, J. J. Optimal Bicelle Size *q* for Solution NMR Studies of the Protein Transmembrane Partition. *Chem. - Eur. J.* **2017**, *23*, 1361−1367.
(17) Mäler, L. Solution NMR studies of cell-penetrating peptides in model membrane systems. *Adv. Drug Delivery Rev.* **2013**, *65*, 1002−1011.
(18) Diller, A.; Loudet, C.; Aussenac, F.; Raffard, G.; Fournier, S.; Laguerre, M.; Grélard, A.; Opella, S. J.; Marassi, F. M.; Dufourc, E. J. Bicelles: A natural 'molecular goniometer' for structural, dynamical and topological studies of molecules in membranes. *Biochimie* **2009**, *91*, 744−751.
(19) Rubio, L.; Rodríguez, G.; Barbosa-Barros, L.; Alonso, C.; Cócera, M.; de la Maza, A.; Parra, J. L.; López, O. Bicellar systems as a new colloidal delivery strategy for skin. *Colloids Surf., B* **2012**, *92*, 322−326.
(20) Rodríguez, G.; Rubio, L.; Cócera, M.; Estelrich, J.; Pons, R.; de la Maza, A.; López, O. Application of Bicellar Systems on Skin: Diffusion and Molecular Organization Effects. *Langmuir* **2010**, *26*, 10578−10584.
(21) Kang, C.; Vanoye, C. G.; Welch, R. C.; Van Horn, W. D.; Sanders, C. R. Functional Delivery of a Membrane Protein into Oocyte Membranes Using Bicelles. *Biochemistry* **2010**, *49*, 653−655.
(22) Lin, L.; Wang, X.; Guo, Y.; Ren, K.; Li, X.; Jing, L.; Yue, X.; Zhang, Q.; Dai, Z. Hybrid bicelles as a pH-sensitive nanocarrier for hydrophobic drug delivery. *RSC Adv.* **2016**, *6*, 79811−79821.
(23) Barbosa-Barros, L.; Rodríguez, G.; Barba, C.; Cócera, M.; Rubio, L.; Estelrich, J.; López-Iglesias, C.; de la Maza, A.; López, O. Bicelles: Lipid Nanostructured Platforms with Potential Dermal Applications. *Small* **2012**, *8*, 807−818.
(24) Barbosa-Barros, L.; de la Maza, A.; Estelrich, J.; Linares, A. M.; Feliz, M.; Walther, P.; Pons, R.; López, O. Penetration and Growth of DPPC/DHPC Bicelles Inside the Stratum Corneum of the Skin. *Langmuir* **2008**, *24*, 5700−5706.
(25) Reijmar, K.; Edwards, K.; Andersson, K.; Agmo Hernandez, V. Characterizing and Controlling the Loading and Release of Cationic Amphiphilic Peptides onto and from PEG-Stabilized Lipodisks. *Langmuir* **2016**, *32*, 12091−12099.
(26) Zhu, L.; Kate, P.; Torchilin, V. P. Matrix Metalloprotease 2-Responsive Multifunctional Liposomal Nanocarrier for Enhanced Tumor Targeting. *ACS Nano* **2012**, *6*, 3491−3498.
(27) Kolate, A.; Baradia, D.; Patil, S.; Vhora, I.; Kore, G.; Misra, A. PEG - A versatile conjugating ligand for drugs and drug delivery systems. *J. Controlled Release* **2014**, *192*, 67−81.
(28) Kooijmans, S.A.A.; Fliervoet, L.A.L.; van der Meel, R.; Fens, M.H.A.M.; Heijnen, H.F.G.; van Bergen en Henegouwen, P.M.P.; Vader, P.; Schiffelers, R.M. PEGylated and targeted extracellular vesicles display enhanced cell specificity and circulation time. *J. Controlled Release* **2016**, *224*, 77−85.
(29) Suk, J. S.; Xu, Q.; Kim, N.; Hanes, J.; Ensign, L. M. PEGylation as a strategy for improving nanoparticle-based drug and gene delivery. *Adv. Drug Delivery Rev.* **2016**, *99*, 28−51.
(30) Saw, P. E.; Yu, M.; Choi, M.; Lee, E.; Jon, S.; Farokhzad, O. C. Hyper-cell-permeable micelles as a drug delivery carrier for effective cancer therapy. *Biomaterials* **2017**, *123*, 118−126.
(31) Zalipsky, S.; Hansen, C. B.; Lopes de Menezes, D. E.; Allen, T. M. Long-circulating, polyethylene glycol-grafted immunoliposomes. *J. Controlled Release* **1996**, *39*, 153−161.
(32) Sandström, M. C.; Johansson, E.; Edwards, K. Influence of preparation path on the formation of discs and threadlike micelles in DSPE-PEG_{2000}/lipid systems. *Biophys. Chem.* **2008**, *132*, 97−103.
(33) Johnsson, M.; Edwards, K. Liposomes, Disks, and Spherical Micelles: Aggregate Structure in Mixtures of Gel Phase Phosphatidylcholines and Poly(Ethylene Glycol)-Phospholipids. *Biophys. J.* **2003**, *85*, 3839−3847.
(34) Johansson, E.; Lundquist, A.; Zuo, S.; Edwards, K. Nanosized bilayer disks: Attractive model membranes for drug partition studies. *Biochim. Biophys. Acta, Biomembr.* **2007**, *1768*, 1518−1525.
(35) Zetterberg, M. M.; Ahlgren, S.; Agmo Hernandez, V.; Parveen, N.; Edwards, K. Optimization of lipodisk properties by modification of the extent and density of the PEG corona. *J. Colloid Interface Sci.* **2016**, *484*, 86−96.
(36) Lundquist, A.; Wessman, P.; Rennie, A. R.; Edwards, K. Melittin−Lipid interaction: A comparative study using liposomes, micelles and bilayer disks. *Biochim. Biophys. Acta, Biomembr.* **2008**, *1778*, 2210−2216.
(37) Liu, Y.; Li, M.; Yang, Y.; Xia, Y.; Nieh, M.-P. The effects of temperature, salinity, concentration and PEGylated lipid on the spontaneous nanostructures of bicellar mixtures. *Biochim. Biophys. Acta, Biomembr.* **2014**, *1838*, 1871−1880.
(38) Yang, P.-W.; Lin, T.-L.; Lin, T.-Y.; Yang, C.-H.; Hu, Y.; Jeng, U-S. Packing DNA with disc-shaped bicelles. *Soft Matter* **2013**, *9*, 11542−11548.
(39) Glover, K. J.; Whiles, J. A.; Wu, G.; Yu, N.-j.; Deems, R.; Struppe, J. O.; Stark, R. E.; Komives, E. A.; Vold, R. R. Structural Evaluation of Phospholipid Bicelles for Solution-State Studies of Membrane-Associated Biomolecules. *Biophys. J.* **2001**, *81*, 2163−2171.
(40) Mortensen, H. G.; Jensen, G. V.; Hansen, S. K.; Vosegaard, T.; Pedersen, J. S. Structure of Phospholipid Mixed Micelles (Bicelles) Studied by Small-Angle X-ray Scattering. *Langmuir* **2018**, *34*, 14597−14607.
(41) Akiba, I.; Terada, N.; Hashida, S.; Sakurai, K.; Sato, T.; Shiraishi, K.; Yokoyama, M.; Masunaga, H.; Ogawa, H.; Ito, K.; Yagi, N. Encapsulation of a Hydrophobic Drug into a Polymer-Micelle Core Explored with Synchrotron SAXS. *Langmuir* **2010**, *26*, 7544−7551.
(42) Manet, S.; Lecchi, A.; Impéror-Clerc, M.; Zholobenko, V.; Durand, D.; Oliveira, C. L. P.; Pedersen, J. S.; Grillo, I.; Meneau, F.; Rochas, C. Structure of Micelles of a Nonionic Block Copolymer Determined by SANS and SAXS. *J. Phys. Chem. B* **2011**, *115*, 11318−11329.
(43) Jeng, U.-S.; Su, C. H.; Su, C.-J.; Liao, K.-F.; Chuang, W.-T.; Lai, Y.-H.; Chang, J.-W.; Chen, Y.-J.; Huang, Y.-S.; Lee, M.-T.; Yu, K.-L.; Lin, J.-M.; Liu, D.-G.; Chang, C.-F.; Liu, C.-Y.; Chang, C.-H.; Liang, K. S. A small/wide-angle X-ray scattering instrument for structural characterization of air−liquid interfaces, thin films and bulk specimens. *J. Appl. Crystallogr.* **2010**, *43*, 110−121.
(44) Kline, S. R. Reduction and analysis of SANS and USANS data using IGOR Pro. *J. Appl. Crystallogr.* **2006**, *39*, 895−900.
(45) Teixeira, J. Small-angle scattering by fractal systems. *J. Appl. Crystallogr.* **1988**, *21*, 781−785.
(46) Hammouda, B. A new Guinier−Porod model. *J. Appl. Crystallogr.* **2010**, *43*, 716−719.
(47) Percus, J. K.; Yevick, G. J. Analysis of Classical Statistical Mechanics by Means of Collective Coordinates. *Phys. Rev.* **1958**, *110*, 1−13.
(48) Chen, S.-H.; Lin, T.-L. Colloidal Solutions. *Methods Exp. Phys.* **1987**, *23B*, 489−543.
(49) Johnsson, M.; Hansson, P.; Edwards, K. Spherical Micelles and Other Self-Assembled Structures in Dilute Aqueous Mixtures of Poly(Ethylene Glycol) Lipids. *J. Phys. Chem. B* **2001**, *105*, 8420−8430.

DOI: 10.1021/acs.langmuir.9b00756
Langmuir 2019, 35, 9483−9492

(50) Tanford, C. Micelle Shape and Size. *J. Phys. Chem.* **1972**, *76*, 3020−3024.
(51) Wu, H.; Su, K.; Guan, X.; Sublette, M. E.; Stark, R. E. Assessing the size, stability, and utility of isotropically tumbling bicelle systems for structural biology. *Biochim. Biophys. Acta, Biomembr.* **2010**, *1798*, 482−488.
(52) Beaugrand, M.; Arnold, A. A.; Hénin, J.; Warschawski, D. E.; Williamson, P. T. F.; Marcotte, I. Lipid Concentration and Molar Ratio Boundaries for the Use of Isotropic Bicelles. *Langmuir* **2014**, *30*, 6162−6170.
(53) Triba, M. N.; Warschawski, D. E.; Devaux, P. F. Reinvestigation by Phosphorus NMR of Lipid Distribution in Bicelles. *Biophys. J.* **2005**, *88*, 1887−1901.

DOI: 10.1021/acs.langmuir.9b00756
Langmuir 2019, 35, 9483−9492